Journal of *Functional Biomaterials*

MDPI

Article

Green Ultrasound-Assisted Synthesis of Surface-Decorated Nanoparticles of Fe_3O_4 with Au and Ag: Study of the Antifungal and Antibacterial Activity

Álvaro de Jesús Ruíz-Baltazar [1,*], Harald Norbert Böhnel [2], Daniel Larrañaga Ordaz [3], José Antonio Cervantes-Chávez [4], Néstor Méndez-Lozano [5] and Simón Yobanny Reyes-López [6,*]

1 CONAHCYT-Centro de Física Aplicada y Tecnología Avanzada, Universidad Nacional Autónoma de México, Boulevard Juriquilla 3001, Santiago de Querétaro 76230, Mexico
2 Centro de Geociencias, Universidad Nacional Autónoma de México, Boulevard Juriquilla 3001, Santiago de Querétaro 76230, Mexico; hboehnel@geociencias.unam.mx
3 Minnesota Dental Research Center for Biomaterials and Biomechanical, School of Dentistry of Minnesota, Minneapolis, MN 55455, USA; daniel.larranaga@outlook.es
4 Unidad de Microbiología Básica y Aplicada, Facultad de Ciencias Naturales, UAQ Campus Aeropuerto, Santiago de Querétaro 76140, Mexico; cervanteschavez@gmail.com
5 Campus Querétaro, Universidad del Valle de México, Blvd. Juriquilla no. 1000 A. Del. Santa Rosa Jáuregui, Querétaro 76230, Mexico; nestor.mendez@uvmnet.edu
6 Instituto de Ciencias Biomédicas, Departamento de Ciencias Químico-Biológicas, Universidad Autónoma de Ciudad Juárez, Anillo Envolvente del Pronaf y Estocolmo s/n, Zona Pronaf, Ciudad Juárez 32310, Mexico
* Correspondence: aruizbaltazar@fata.unam.mx (Á.d.J.R.-B.); simon.reyes@uacj.mx (S.Y.R.-L.)

Abstract: This work proposes a sonochemical biosynthesis of magnetoplasmonic nanostructures of Fe_3O_4 decorated with Au and Ag. The magnetoplasmonic systems, such as Fe_3O_4 and Fe_3O_4-Ag, were characterized structurally and magnetically. The structural characterizations reveal the magnetite structures as the primary phase. Noble metals, such as Au and Ag, are present in the sample, resulting in a structure-decorated type. The magnetic measurements indicate the superparamagnetic behavior of the Fe_3O_4-Ag and Fe_3O_4-Au nanostructures. The characterizations were carried out by X-ray diffraction and scanning electron microscopy. Complementarily, antibacterial and antifungal assays were carried out to evaluate the potential properties and future applications in biomedicine.

Keywords: magnetic nanoparticles; magnetoplasmonic; antibacterial; antifungal; green synthesis; sonochemistry

check for updates

Citation: Ruíz-Baltazar, Á.d.J.; Böhnel, H.N.; Larrañaga Ordaz, D.; Cervantes-Chávez, J.A.; Méndez-Lozano, N.; Reyes-López, S.Y. Green Ultrasound-Assisted Synthesis of Surface-Decorated Nanoparticles of Fe_3O_4 with Au and Ag: Study of the Antifungal and Antibacterial Activity. *J. Funct. Biomater.* **2023**, *14*, 304. https://doi.org/10.3390/jfb14060304

Academic Editors: Zhou Ye and Ting Sang

Received: 9 May 2023
Revised: 23 May 2023
Accepted: 25 May 2023
Published: 1 June 2023

1. Introduction

Nowadays, the research and development of magnetoplasmonic nanostructures have been widely studied due to their multiples applications in fields, such as catalysis, magneto-optics devices, energy storage, biosensors, drug delivery, photocatalysis, cancer treatment, hyperthermia, among others [1–3]. Commonly, magnetoplasmonic structures are constituted by ferromagnetic materials and noble metals, generally, gold and silver, as their remarkable properties are exhibited individually. In this sense, the catalytic, antibacterial, antifungal, biocompatible, and optoelectronic properties of noble metals, such as Ag and Au, allow them to be used in multiple fields, such as biomedicine, water treatment, catalysis, and photocatalysis, among others. Additionally, Au and Ag have been employed as electrochemical sensors, biosensors, and antibacterial and antifungal materials [4–9].

Concerning ferromagnetic materials, the superparamagnetic iron oxides nanoparticle's (SPION's) materials are the most commonly employed. The wide range of properties exhibited by the SPIONs allows their use in fields, such as medicine, optics, electronics, biology, and catalysis. However, the potentials applications of the magnetoplasmonic nanostructures depend directly on their morphology and size [4,10–12].

On the one hand, plasmonic materials, such as gold and silver, have been widely used due to their high biocompatibility and chemical and physical properties, which can promote mechanisms for the detection of components of biological interest. In addition, noble metals exhibit low toxicity, non-immunogenicity, and hydrophilicity and can be employed for selective drug delivery. Furthermore, the key optical features of the Au nanoparticles, such as surface plasmon resonance (SPR), SERS, and luminescence, allow gold nanoparticles to be used as biosensors and biomarkers. Specifically, the sensing mechanisms of the biosensors based on Au nanoparticles are supported by an optical phenomenon associated with the interaction between the conduction band of the Ag nanoparticles and the light photons, resulting in a conjunct oscillation of the ultraviolet–visible band and the valence electrons (SPR) [13–15]. In the case of the SERS methodology, it is based on an amplification of Raman scattering of the specific molecules absorbed on the metallic nanostructures or rough metal surfaces [16]. On the other hand, the magnetic materials, such as the SPION's, the magnetic properties and functionality of these species have generated multiple applications in magnetic resonance imaging (MRI), specifically as magnetic contrast agents [17]. In this sense, new researchers are focused on developing nanostructures with iron oxide cores and some coatings or shells with hydrophilic properties with the finality to increase the magnetic susceptibility and consequently, their functionality [18]. Another important aspect is the kind of iron oxide employed in active targeting applications; the most common and functional iron oxides are magnetite (Fe_3O_4) and/or maghemite (γFe_2O_3) due to providing the particles with a magnetic resonance detectable signal, and the magnetic properties are similar to both species [19]. Likewise, the SPION's size is directly related to its characteristic superparamagnetic behavior. It can be explained from the point of view of the aligned unpaired electrons spins (oriented magnetic domains), which depending on the structure and size of the SPION, can be classified as superparamagnetic if the material presents single domain crystals and exhibits a significantly larger magnetic susceptibility [20–22].

In this sense, the design and synthesis of magnetoplasmonic nanostructures acquire a preponderant place in nanotechnology. For this reason, the development of synthesis routes that lead obtains homogeneous structures in composition, morphology, and size and nowadays is an interesting topic [23–25]. In this regard, the implementation and search for ecological alternatives for the synthesis of nanostructures has been focused on green chemistry due to these methodologies to eliminate or significantly reduce the use and generation of toxic chemical reagents and hazardous substances [26–29]. The green synthesis of nanostructures is commonly based on the use of extracts from plants, bacteria, algae, fungi, roots, and yeasts, among others, as reducing agents during green synthesis [4,30,31]. This is due to the nanostructures containing high levels of antioxidants, phenolic compounds, flavonoids, isoflavones flavanones, flavones, flavanols, and anthocyanidins [17–19]. Additionally, the implementation of ultrasound-assisted green synthesis represents a great alternative for obtaining bifunctional system nanostructures composed of SPIONs, Au, and Ag [19,25,32].

In concrete form, the sonochemical synthesis of magneto plasmonic nanoparticles promotes the dispersion of the reactive and reactants during the synthesis process. Many reports indicate that it is possible to obtain bifunctional systems, such as those composed by SPIONs, Au, and Ag [22,33,34], through sonochemical synthesis.

On the other hand, the biomedical applications of magnetoplasmonic materials have been accentuated, specifically in the antibacterial and antifungal fields, due to the actual threats in health topics due to bacterial multidrug resistance. This is derivative to the excessive and imprudent use of antibiotics complicating the control of the epidemic [18,35]. In this sense, the increasing rate of microbial resistance has propelled and motived the search for and development of efficient therapies. In this regard, the incorporation of phytochemicals contained in plants, also known as organic antibiotics, have exhibited significant antibacterial properties. According to their organic compounds, the organic antibiotics can be classified as alkaloids, terpenoids, polyphenols, and sulfur-containing compounds [35,36]. These compounds are commonly found on plants, such as *Berberis*

vulgaris, *Piper nigrum*, *Arctium lappa*, *Carum carvi*, *Rhamnus purshiana*, *Matricaria chamomilla*, *Eucalyptus globulus*, among others. Specifically, components derived from the alkaloids, such as reserpine, piperine, berberine, chanoclavine, conessine, solasodine, evocarpine, and tomatidine, hves shown exceptional results against *Staphylococcus aureus*, *Streptococcus agalactiae*, *Micrococcus luteus*, and *Escherichia coli*, among others. Regarding the terpene compounds, for instance, farnesol, nerolidol, and dehydroabietic acid, it has been observed that these compounds manage to generate a cell membrane disturbance against *S. aureus* bacteria [18,35]. In addition, phenolic compounds, such as resveratrol, baicalein, biochanin a and formononetin, have shown reductions in the minimum inhibitory concentration values of antibacterial agent against mycobacterium smegmatis and campylobacter jejuni, among others. Other important eukaryotic pathogens, such as the fungi, also show a threat due to their intrinsic characteristics of adaptations in metabolism and morphogenesis that enable fungi to generate problems in human health. It has been reported that eukaryotic microorganisms, such as phylum Ascomycota specie, contain virulent fungi, such as coccidioides, coccidioides, clastomyces, histoplasma, scedosporium, fusarium, aspergillus, and candida species [4,37].

The latter species is a priority study objective since most human infections caused by fungal pathogens are attributed to this species, specifically, *Candida albicans*, *Candida glabrata*, which exhibits significant drug resistance, and *Candida auris*, which has recently been considered the new threat to global public health. Furthermore, emerging species, such as *Candida krusei*, *Candida tropicalis*, and *Candida parapsilosis*, have also generated particular interest [37].

Based on the above arguments, it is necessary to develop alternatives to address this problem. Nanoparticles (NPs) of noble metals and metal oxides have proven to be functional alternatives to address antibiotic and antifungal problems. In this regard, the use of this systems in antibacterial and antifungal applications has been widely reported recently due to actually slowing the approved rate of antibiotics and antifungals [4,38–41]. Systems composed of iron oxides, Au, and Ag nanoparticles have been probed again microorganism, such as *E. coli*, *S. aureus*, *Candida parapsilosis*, *C. glabrata*, and *C. albicans* [3,5,42]. Because these types of nanoparticles can penetrate the cell membranes in bacteria and fungi, altering cell function, on the other hand, the high surface energy of the particles promotes the antibacterial and antifungal effect [4,43–45].

This work intends to focus on the problem of the resistance of bacteria and fungi to traditional antibiotics, generating novel alternatives from the point of view of the synthesis of the proposed materials, which are obtained through the use of green chemistry. Emphasizing the innovation of the green methodology, which offers an alternative considerably more economical and ecological, since the use of organic extracts, such as *Piper auritum,* during the synthesis methodology of magnetoplasmonic nanostructures and the use of ultrasound as a complementary tool allows us to propose a hybrid and functional methodology for obtaining this type of nanostructures.

The use of magnetoplasmonic materials are novel due to their broad and synergistic properties (plasmonic and magnetic). The structural and chemical characterization confirms the synthesis of the Fe_3O_4, Fe_3O_4-Au, and Fe_3O_4–Ag structures. The antibacterial and antifungal activities of the obtained nanostructure were evaluated against Gram-positive bacteria, *Staphylococcus aureus* (ATCC 6538), and *Escherichia coli* (ATCC 8739) as Gram-negative. For eukaryotic, yeast cells of *Candida parapsilosis*, *C. glabrata*, and *C. albicans* (ATCC 10231) were selected. Significant results were found regarding the antibacterial and antifungal activities of the Fe_3O_4-Au and Fe_3O_4-Ag samples. The synergistic effect of noble metals with iron oxides as an antifungal and antibacterial alternative is presented and discussed in this work.

2. Materials and Methods

2.1. Green Synthesis of Magneto-Plasmonic Systems

The synthesis of the magnetoplasmonic systems (Fe_3O_4, Fe_3O_4-Au, and Au-Ag) were carried out from *Piper auritum* extract and assisted by ultrasound. In the case of the Fe_3O_4 nanoparticles, a FeCl3.6H_2O/FeCl2.4H2O solution in a ratio of Fe (III)/Fe (II):2 was employed as the precursor agent. The reducing agent from the Piper auritum extract were obtained with a mixture of 200 mL of deionized water with 15 g of Piper auritum leaves. The mixture obtained was heated at 100 °C for 10 min.

The synthesis of Fe_3O_4-Au nanoparticles was carried out in an analogous form to the methodology reported in a previous work [24]. Briefly, the reducing agent from the *Piper auritum* extract was obtained with a mixture of 200 mL of deionized water with 15 g of *Piper auritum* leaves. The mixture obtained was heated at 100 °C for 10 min. On the other hand, the metallic precursor was prepared with a $HAuCl_4 \cdot 3H_2O$ solution at 50 mM. Posteriorly, the precursor and the reducing agent were mixed and ultrasonicated at 42 kHz for 15 min. Finally, a $FeCl_3.6H_2O$/$FeCl_2.4H_2O$ solution in a ratio of Fe (III)/Fe (II):2 was added to the previous mixture and assisted with ultrasonic agitation for 60 min. (Digital Ultrasonic Cleaner, Brand: Kendall, Model: CD-4820, Pontiac, MI 48341, USA; 42 kHz of frequency and 160 W). The pH of the synthesis reaction was adjusted to 11 by adding a NaOH solution. The Fe_3O_4-Au nanoparticles obtained were washed in an isopropyl alcohol solution and centrifuged. The colloidal solution of the Fe_3O_4-Au nanoparticles was dried for the subsequent procedures of the chemical–structural characterization and properties evaluations. On the other hand, the Fe_3O_4-Ag nanoparticles were obtained in similar form of Fe_3O_4-Au nanoparticles. In this case, a solution of $AgNO_3$ at 50 mM was employed as a precursor. This solution was mixed and sonicated with the reducing agent (*Piper auritum* extract). Posteriorly, a previously prepared $FeCl_3.6H_2O$/$FeCl_2.4H_2O$ solution was added to the precursor/reducing agent solution. In the final stage of the process, the mix obtained was heated at 40 °C under ultrasonic agitation for 60 min. The solution obtained was washed with isopropyl alcohol and centrifuged at 4000 rpm for a period of 15 min. (Thermo Scientific brand, Waltham, MA, USA; Heraeus X1R model) at 4 °C. In the final stage, the solution was decanted, and the solids obtained were lyophilized.

2.2. X-ray Diffraction Analysis

The structural characterization of the Fe_3O_4, Fe_3O_4-Au and Au-Ag samples were carried out in a Rigaku Ultima IV X-ray diffractometer (Suite 475 Austin, TX 78717, USA). In a range of exploration of 10–80 degrees (2θ) with Cu-Kα radiation (λ = 1.54° A). The step of the analysis was 5° per minute and sampling every 0.02.

2.3. Scanning Electron Microscopy (SEM)

The morphology and the configuration of the Fe_3O_4, Fe_3O_4-Au, and Au-Ag samples were determined by high-resolution scanning electron microscopy (HRSEM) through a Hitachi SU-8230 Scanning Electron Microscope (2535 Augustine Drive, Santa Clara, CA 95054, USA). The microscope was equipped with a cold field emission device.

2.4. Chemical Characterization

The chemical composition of the samples was determined by energy-dispersive X-ray spectroscopy (EDS). The elemental compositions of the samples were collected with a Bruker X Flash 6/60 system coupled to the Hitachi SU-8230 Scanning Electron Microscope.

2.5. Antibiotic Assay

In order to determine if the magnetite nanoparticles showed antimicrobial activity, we tested its effect by means of the Kirby Bauer method using procaryotic and eukaryotic cells. Briefly, 5 mg of nanoparticles S7, S14, and S15 were weighed independently, and 1 mL of distilled water was added to each one. As a Gram-positive representative bacteria we chose *Staphylococcus aureus* (ATCC 6538) and *Escherichia coli* (ATCC 8739) as a Gram-

negative representative bacteria. For eukaryotic, yeast cells of *Candida parapsilosis*, *C. glabrata* (kindly donated by Elva T. Aréchiga Carvajal, Universidad Autónoma de Nuevo León) and *C. albicans* (ATCC 10231) were selected.

Bacteria strains were grown in nutrient broth (NB) media and were incubated at 37 °C for 20 h. For yeast, YPD (2% yeast extract, 1% peptone 2% dextrose) media was used and were incubated at 28 °C for 24 h. Optical density (OD) was scored at 595 nm (Thermo Scientific Genesys 105-UV-Vis). Then, OD of the cultures was adjusted to 1 OD unit using fresh NB or YPD media. Next, a volume of 200 µL was spread with the aid of sterile glass beads on Muller Hinton agar (bacteria) or YPD (yeast). Later on, filter disks of Whatman paper were placed on the plates, and 100 µL of each nanoparticle were dispensed. As the control, a volume of 100 µL of sterile distilled water was dispensed on a filter paper disk. Plates were dry in the hood, then incubated at 37 °C (bacteria) or 28 °C (yeast) for 24 h. Next, the inhibition halo sizes were measured, and plates were photographed. Experiments were conducted by triplicate. Data were analyzed by one way ANOVA.

3. Results and Discussion

3.1. Materials Characterization

Scanning Electron Microscopy

The scanning electron microscopy SEM (HA-T) of the Fe_3O_4 is shown in Figure 1a, which indicates the semispherical morphology and a high agglomeration degree. This fact can be attributed to the strong interaction generated on the Fe_3O_4 nanoparticles surface. On the other hand, the distribution particle size observed was 35 nm approximately. The subsequent X-ray diffraction analysis complements the crystallite size of the samples. Figure 1b shows in detail a SE image of the Fe_3O_4 sample. In this image, the semispherical morphology, the particle distribution size, and the agglomeration of the Fe_3O_4 NPs are corroborated. The Energy dispersive spectroscopy (EDS) mapping of the Fe_3O_4 is presented in Figure 1c. The constitutive elements (Fe and O) of the Fe_3O_4 NPs were fully identified and marked. In complementary form, Figure 1d,e, illustrate the elemental mapping of the oxygen an iron, respectively.

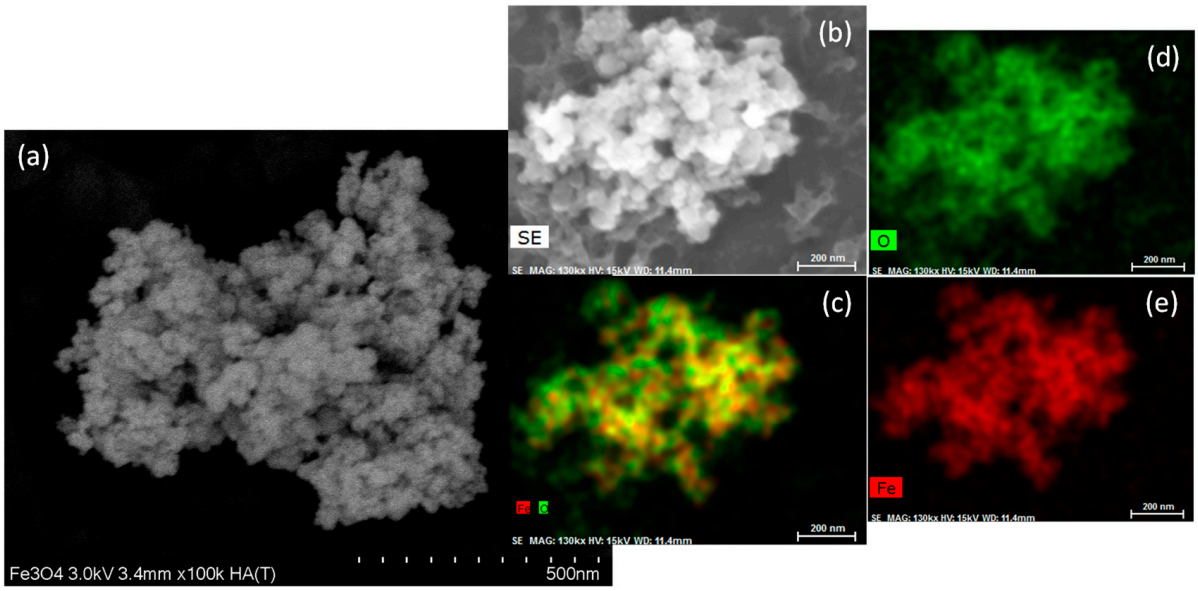

Figure 1. Scanning electron microscopy SEM images of the Fe_3O_4 nanoparticles: (**a**) operated in transmission mode at 3.0 kV, (**b**) secondary electrons image, (**c**) energy dispersive spectrometry (EDS) general mapping(Image sizes are annotated by the scale bar in the lower right corner of the respective image), and (**d**,**e**) elemental mapping of oxygen and iron, respectively.

In regard to the Fe_3O_4-Ag NPs, Figure 2a shows an SEM image of the sample, where similar characteristics to the Fe_3O_4 sample were observed in terms of morphology, size distribution, and agglomeration degree. However, the silver added to the Fe_3O_4 synthesis showed a partial nucleation on the Fe_3O_4 NPs. Fe_3O_4-Ag NPs are given as the decorated type. The Ag NPs nucleated on the magnetite surface exhibits an approximated size of 25 nm. Figure 2b shows the EDS mapping of the sample Fe_3O_4-Ag, which corroborates the Ag presence. The individual mapping element associated with Ag, O, and Fe are presented in Figure 2c–e, respectively.

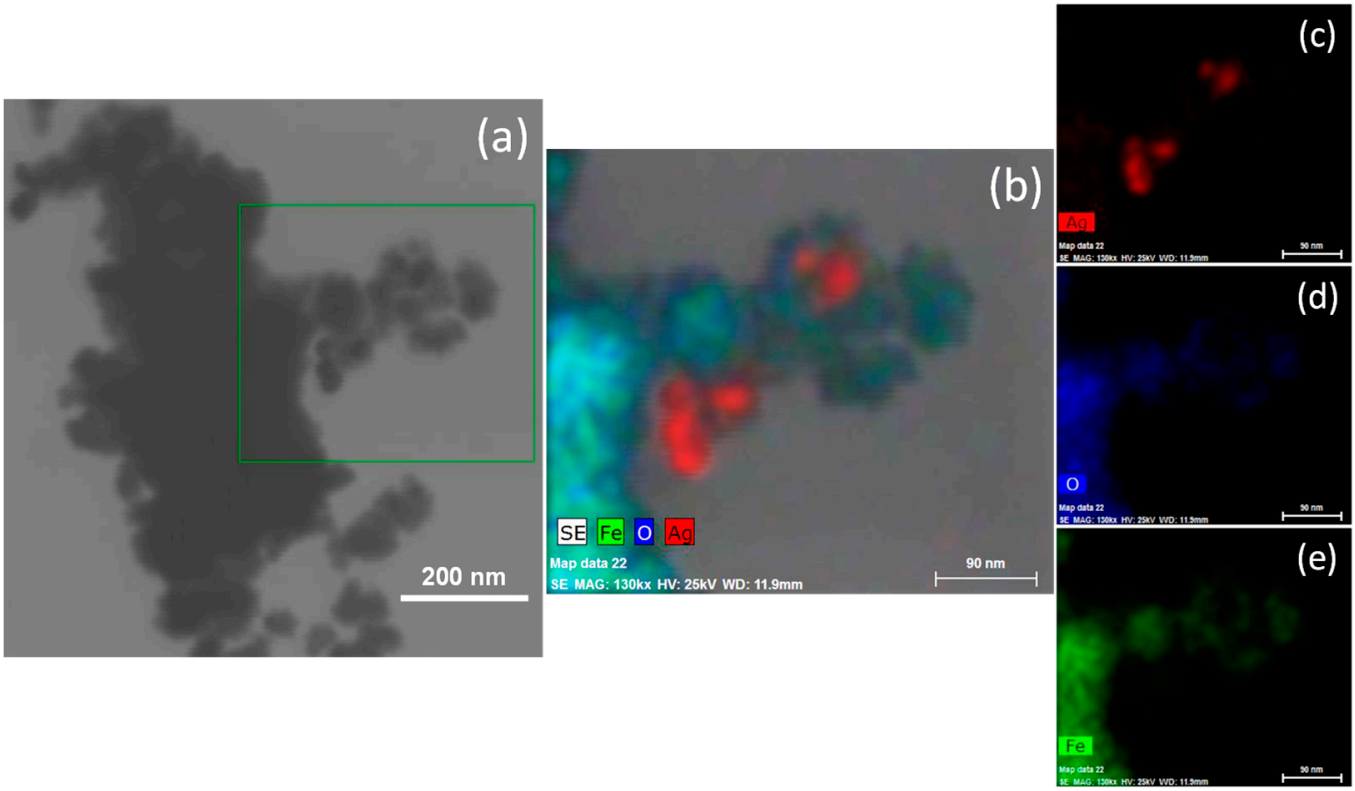

Figure 2. (**a**) SEM micrographs of the Fe_3O_4-Ag plasmonic nanoparticles: (**b**) elemental mapping of the Fe_3O_4-Ag nanostructures obtained, and (**c**–**e**) individual mappings of the Ag, O, and Fe elements, respectively (Image sizes are annotated by the scale bar in the lower right corner of the respective image).

Finally, the structure and morphology of the Fe_3O_4-Au samples are described in Figure 3a–f. Specifically, Figure 3a shows an SEM image of the Fe_3O_4-Au sample, which describe in general form, the distribution and agglomeration degree of the Fe_3O_4-Au NPs. In this figure it is possible to appreciate the Fe_3O_4 and Au configuration as a decorated type. Figure 3b illustrate in detail an individual particle of Fe_3O_4-Au. The specific localizations of the Fe, O, and Au are appreciated (Figure 3c). As part of the chemical characterization, elemental EDs mapping of Fe, Au, and O are showed in Figure 3d–f, respectively.

In this sense, and according to the synthesis method, the Fe_3O_4 act as nucleation sites, which promote the Au NPs growth. For this reason, particles decorated type were obtained.

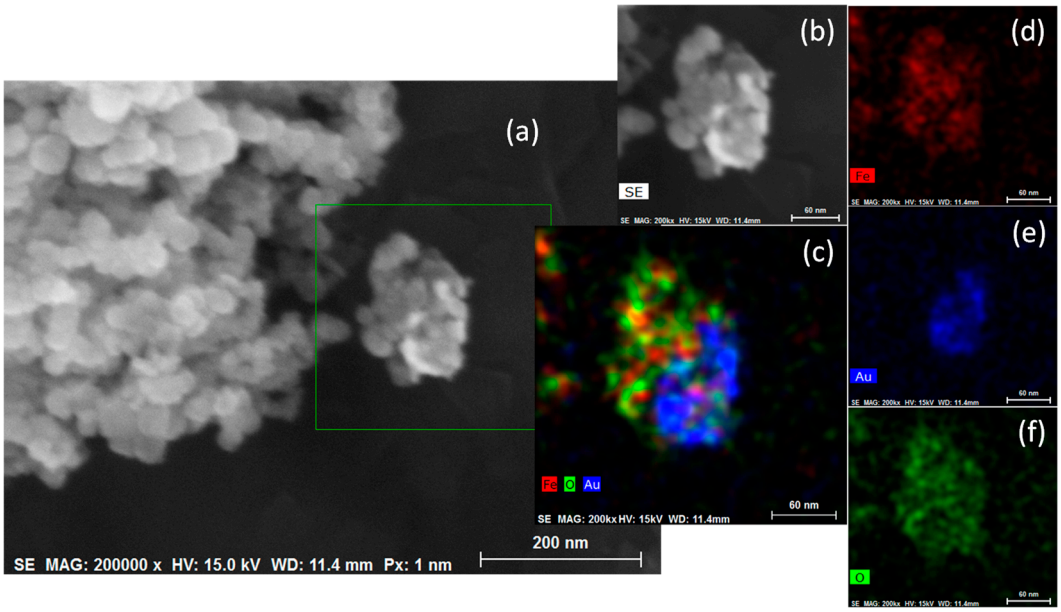

Figure 3. (**a**,**b**) Secondary electron micrographs of the Fe_3O_4-Au nanoparticles: (**c**) EDS mapping of Fe_3O_4-Au sample obtained at 15 kV and (**d**–**f**) elemental mappings of Fe, Au, and O (Image sizes are annotated by the scale bar in the lower right corner of the respective image).

3.2. X-Ray Diffraction Analysis and Williamson-Hall Methods (W-H)

In order to elucidate the structure of the Fe_3O_4, Fe_3O_4-Ag, and Fe_3O_4-Au samples, XRD analysis was carried out. XRD patterns and their respective Williamson–Hall plots are described in Figure 4a–f. In general form, the Williamson–Hall methods can be employed to calculate the crystallite size from the XRD patterns. In this work the uniform deformation model is considered to calculate the crystallite size and strain in the Fe_3O_4, Fe_3O_4-Ag, and Fe_3O_4-Au nanoparticles.

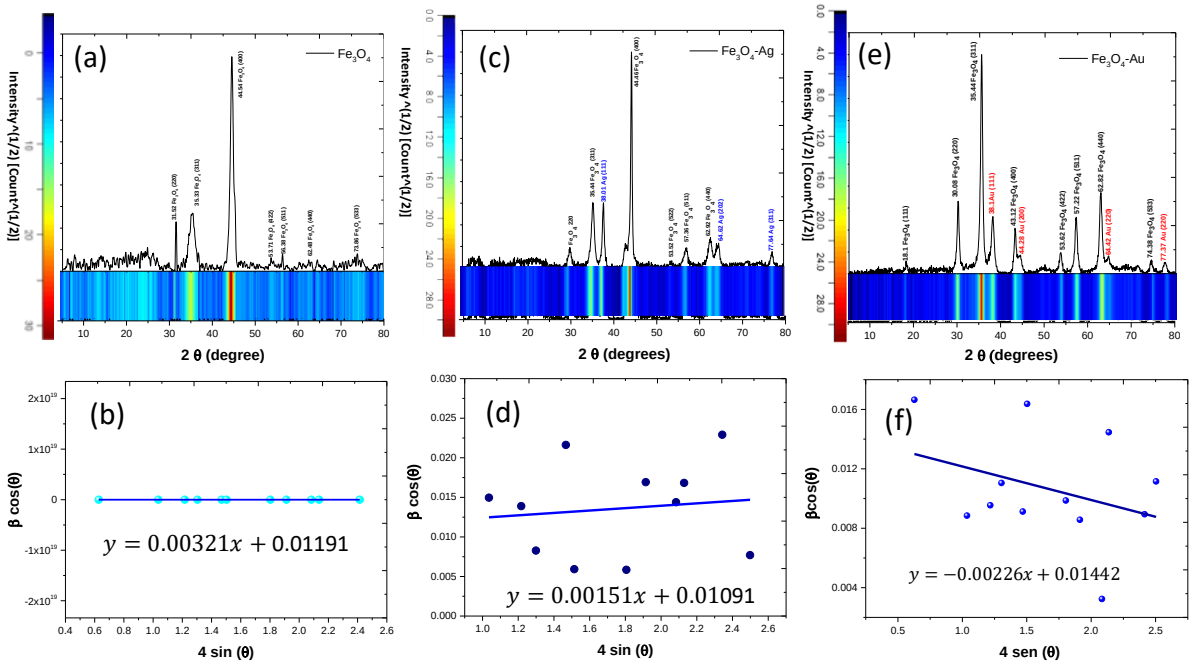

Figure 4. X-ray diffraction patterns and Williamson–Hall plots corresponding to the (**a**,**b**) Fe_3O_4, (**c**,**d**) Fe_3O_4-Ag, and (**e**,**f**) Fe_3O_4-Au nanoparticles.

Uniform Deformation Model (UDM)

In this method, the central idea is the fact that the XRDs are not only influenced by the crystal size but also by the strains and deformations of the crystal lattice of the material. Intrinsically, the W-H analysis is a simplified integral breadth method through which it is possible to discern between the peaks induced by deformation and the peaks associated with the crystallite sizes. In this sense, the individual contributions observed on the line broadening in the diffraction angle (2θ) can be expressed as [46,47]:

$$\beta_{hkl} = \beta_s + \beta_D \quad (1)$$

where β_{hkl} is the full width at half maximum (FWHM) of the observed peaks in the X-ray diffraction patterns. Consequently, βs and β_D are the contributions to the width peak attributed to the size and strain, respectively. It is assumed that the strain is uniform throughout a specific crystallographic direction. The mathematical expression for the uniform deformation model (UDM) is defined as [47,48]:

$$\beta_{hkl} = \frac{k\lambda}{D\cos\theta} + 4\varepsilon\tan\theta \quad (2)$$

Rewriting Equation (3):

$$\beta_{hkl}\cos\theta = \frac{k\lambda}{D} + 4\varepsilon\sin\theta \quad (3)$$

Based on Equation (4), the values of $\beta\cos\theta$ and $4\sin\theta$ can be graphed from the linear fit and the respective slope and intercept can be used to calculate the crystallite size and strain of the samples, respectively. Figure 2b,d,f show the (UDM) of the Fe_3O_4, Fe_3O_4-Ag, and Fe_3O_4-Au, respectively.

From the obtained values of the slope and intercept in the Williamson–Hall plots, the crystallite sizes calculated are 12.93, 14.12, and 10.58 nm for the Fe_3O_4, Fe_3O_4-Ag, and Fe_3O_4-Au NPs, respectively. These results are consistent with the SEM images. Nevertheless, the plasmonic systems show a high agglomeration degree; nonetheless, in the SEM image it is possible to observe individual particulates with crystallite sizes approximate to the calculated values by the Williamson–Hall methods. Therefore, it is possible to affirm that the theoretical calculations associated with the crystallite sizes can describe and confirm the sizes distribution of the nanoparticles observed by SEM. With respect to the synthesis methodology, it is possible to affirms that the Fe_3O_4, Fe_3O_4-Au, and Fe_3O_4-Ag structures are formed by the ultrasound-assisted methodology and the use of the Piper auritum extract as the reducing agent. The nucleation rates of the iron, gold, and silver, as well as the reaction time are consistent with the Fe_3O_4, Fe_3O_4-Au and Fe_3O_4-Ag obtention. The configuration surface-decorated nanoparticles are fully identified and are confirmed chemical and structurally. The following magnetic measures presented can confirm the magnetic behavior as a function of the SPION's type obtained.

3.3. Magnetic Properties

In order to establish the magnetic behavior of the Fe_3O_4, Fe_3O_4-Ag, and Fe_3O_4-Au NPs, hysteresis loop of the materials were carried out. Figure 5a–f show graphically the magnetic properties observed for each sample. Specifically, Figure 5a,c,e describe the hysteresis loop from the Fe_3O_4, Fe_3O_4-Ag, and Fe_3O_4-Au nanoparticles, respectively. Table 1 shows the values of the magnetics parameters, such as saturation magnetization (Ms), remanent magnetization (Mrs), and coercive field associated with the Fe_3O_4, Fe_3O_4-Ag and Fe_3O_4-Au samples.

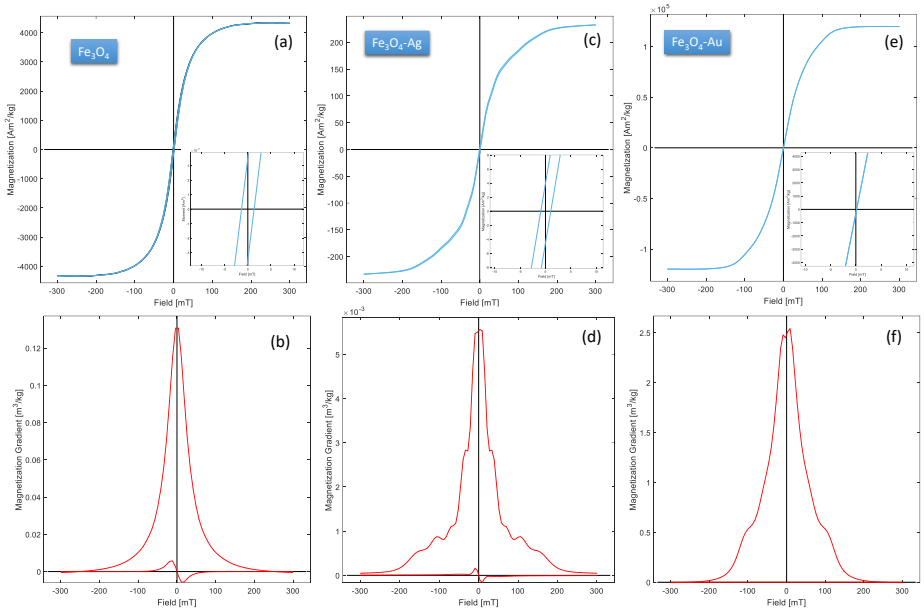

Figure 5. (**a**,**c**,**e**) Hysteresis loops of the Fe_3O_4, Fe_3O_4-Ag, and Fe_3O_4-Au NPs. (**b**,**d**,**f**) Magnetization gradients plots of the magnetoplasmonic systems of Fe_3O_4, Fe_3O_4-Ag, and Fe_3O_4-Au, respectively.

Table 1. Magnetic parameters measured from the Fe_3O_4, Fe_3O_4-Ag, and Fe_3O_4-Au nanoparticles.

Sample	Ms (Am^2/kg)	Mrs (Am^2/kg)	Bc (mT)
Fe_3O_4	4340	147	1.4
Fe_3O_4-Ag	217	4.25	1.0
Fe_3O_4-Au	120,000	304	0.2

In this sense, it is important to note that the Bc value is nearly zero in three cases; consequently, a superparamagnetic behavior can be considered. The incorporation of the noble metals (Ag and Au) to the iron oxide, in this case, promotes a clear tendency to the superparamagnetic behavior of the material. Thus, the observed diminution in the Bc value as a composition function of the samples can be attributed in the first instance to the crystallite size and to the ordering of the nanodomains (magnetic anisotropy) [20,25,49,50]. That is to say, the interactions between the canted spins at the iron oxide surface associated with the crystallite size can determine the superparamagnetic behavior of the Fe_3O_4, Fe_3O_4-Ag, and Fe_3O_4-Au samples. Finally, Figure 5b,d,f, show the magnetization gradients, Mr and Mrs, corresponding to magnetoplasmonic Fe_3O_4, Fe_3O_4-Ag, and Fe_3O_4-Au NPs. These graphs illustrate and support the parameters obtained from the hysteresis loop, where the approximate superparamagnetic behavior is confirmed. On the other hand, the Ms value associated with the Fe_3O_4-Au sample exhibits a considerable increase; this fact can be related to factors, such as magnetic domains, particle sizes, the quantity of Au incorporated to the decorated, and mainly to the synergic effect of the Fe_3O_4 and the Au since the Fe_3O_4-Au NPs are composed of two species, generating regions aligned in the spins on the surface and interface of the particles [33].

3.4. Antibacterial and Antifungal Activity Assay

The Fe_3O_4-Ag and Fe_3O_4-Au nanoparticles showed antibacterial activity against the Gram-positive *S. aureus* and Gram-negative *E. coli* bacteria. *S. aureus* produces infections, such as bacteremia, endocarditis, pneumonia, and sepsis. Similar inhibitory halos were obtained with both kinds of nanoparticles (Figure 6), suggesting a general way of action of

this material, considering the cell wall differences presented between Gram-positive and -negative bacteria [13,51].

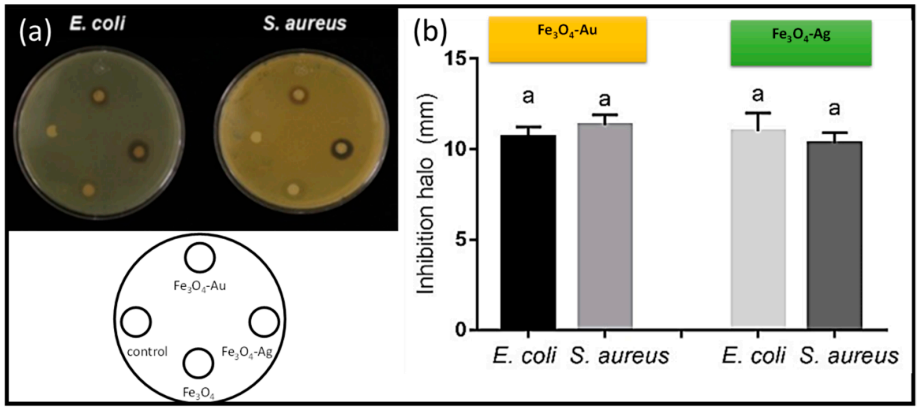

Figure 6. (**a**) Inhibition zone test obtained from the Fe3O4-Ag, and Fe3O4-Au nanoparticles against *S. aureus* and *E. coli* (sample distribution in the antibacterial assays is inserted at the bottom of the image) and (**b**) antibacterial activity graphs of the Fe_3O_4, Fe_3O_4-Ag, and Fe_3O_4-Au nanoparticles against the Gram-positive *S. aureus* and Gram-negative *E. coli* bacteria. (The letters a on the graphs describe the statistical differences between the data).

On the other hand, regarding the fungicide effect of Fe_3O_4 particles in eukaryotic cells, it is important to mention the fact that three Candida species were tested: *C. albicans*, *C. parapsilosis*, and *C. glabrata*, all human-life-threatening pathogens due to the high morbidity and mortality [52,53]. In our experiments, the three species were similarly affected either by Fe_3O_4-Ag or Fe_3O_4-Au nanoparticles (Figure 7). Since the cell wall is the first structure to establish contact with the environment and with the host, it is important to stress the importance of the data obtained with Candida regarding that the cell wall is similar in composition (glucans, mannans, or chitin), but the architecture is different, changing in this way the interaction with the host [54,55].

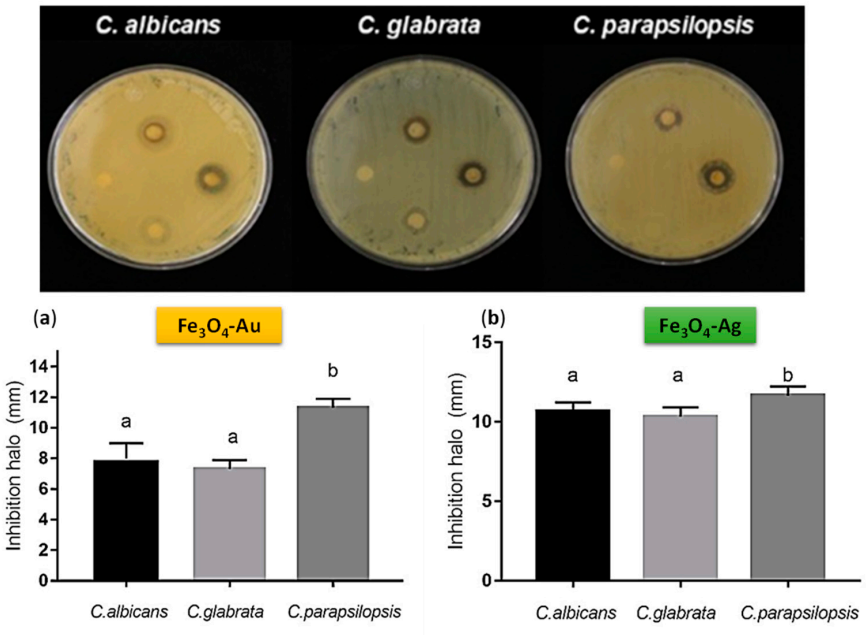

Figure 7. Antifungal activity against *C. albicans*, *C. glabrata*, and *C. parapsilopsis* of the (**a**) Fe_3O_4-Au and (**b**) Fe_3O_4-Ag samples obtained by green synthesis route (The letters a and b on the graphs describe the statistical differences between the data).

Nevertheless, prokaryotic or eukaryotic cells were not affected by the presence of magnetite nanoparticles since no growth inhibition was observed (data not shown), suggesting that the antibiotic effect observed was due to the action of metallic ions or to the interaction between magnetite and the metal. Our results highlight the possibility of using Fe_3O_4-Ag or Fe_3O_4-Au nanoparticles as an alternative approach to control the growth of Candida strains either sensitive or resistant to antibiotics, as well as *S. aureus*. Likewise, these types of nanostructures could be used in dental implants whenever biocompatibility tests are carried out. The high antibacterial and antifungal activity observed by these systems (Fe_3O_4-Au and Fe_3O_4-Ag) offer the possibility to be employed as nanocarriers of drugs in dental applications [56–59].

4. Conclusions

The magnetoplasmonic systems Fe_3O_4- (Ag and Au) synthesized by green route proposed in this work exhibits significant magnetic and antibiotic properties. On the one hand, the nanoparticles obtained by green route structurally show a decorated type in the case of the systems Fe_3O_4-Ag and Fe_3O_4-Au. The structures of the samples were fully identified and associated with Fe_3O_4, Fe_3O_4-Ag and Fe_3O_4-Au. On the other hand, regarding to the magnetic properties of the nanoparticles obtained, a near superparamagnetic behavior was observed in Fe_3O_4, Fe_3O_4-Ag, and Fe_3O_4-Au. Finally, the antibiotics assay shows potential applications of the Fe_3O_4-Ag and Fe_3O_4-Au as antibacterial and antifungal materials. Specifically, our results highlight the possibility to use Fe_3O_4-Ag or Fe_3O_4-Au nanoparticles as alternative approaches to control the growth of Candida strains either sensitive or resistant to antibiotics, as well as *S. aureus*.

This is presumably due to the presence of the metallic nanoparticles and the synergic effect of the magnetite and the noble metals and their respective interactions with the prokaryotic or eukaryotic cells.

Author Contributions: Á.d.J.R.-B. conceptualization; writing—original draft preparation; supervision; project administration; formal analysis; project administration; writing—review and editing. S.Y.R.-L. writing—review and editing; formal analysis, H.N.B. software; methodology; data curation; validation. D.L.O. review and editing; software. J.A.C.-C. methodology; writing—review and editing; data curation; formal analysis. N.M.-L.; software; review and editing; data curation. All authors have read and agreed to the published version of the manuscript.

Funding: National Council of Humanities Sciences and Technologies (CONAHCYT); Project 155 of the Re-searchers for Mexico-CONAHCYT program (IxM).

Institutional Review Board Statement: Not applicable.

Informed Consent Statement: Not applicable.

Data Availability Statement: No new data were created or analyzed in this study. Data sharing is not applicable to this article.

Acknowledgments: Álvaro de Jesús Ruíz-Baltazar and the authors thank the support from the National Council for Science and Technology (CONAHCYT, México) in collaboration with the Center of Applied Physics and Advanced Technology (CFATA-UNAM) through the "Investigadores por México-CONAHCYT" program and the national materials characterization laboratory (LaNCaM) associated with the CFATA-UNAM. Likewise, the authors express our gratitude to the microscopy laboratory (M.C. Manuel Aguilar Franco and Rodrigo Esparza) and to the Basic and Applied Microbiology Unit (UAQ) and the Paleomagnetism Laboratory (CGEO-UNAM, Juriquilla).

Conflicts of Interest: The authors declare no conflict of interest.

References

1. Kandasamy, G.; Maity, D. Multifunctional Theranostic Nanoparticles for Biomedical Cancer Treatments—A Comprehensive Review. *Mater. Sci. Eng. C* **2021**, *127*, 112199. [CrossRef]
2. Lavorato, G.C.; Das, R.; Alonso Masa, J.; Phan, M.H.; Srikanth, H. Hybrid Magnetic Nanoparticles as Efficient Nanoheaters in Biomedical Applications. *Nanoscale Adv.* **2021**, *3*, 867–888. [CrossRef] [PubMed]

3. Huang, J.; Lin, L.; Sun, D.; Chen, H.; Yang, D.; Li, Q. Bio-Inspired Synthesis of Metal Nanomaterials and Applications. *Chem. Soc. Rev.* **2015**, *44*, 6330–6374. [CrossRef]
4. Husain, S.; Nandi, A.; Simnani, F.Z.; Saha, U.; Ghosh, A.; Sinha, A.; Sahay, A.; Samal, S.K.; Panda, P.K.; Verma, S.K. Emerging Trends in Advanced Translational Applications of Silver Nanoparticles: A Progressing Dawn of Nanotechnology. *J. Funct. Biomater.* **2023**, *14*, 47. [CrossRef]
5. Menichetti, A.; Mavridi-printezi, A.; Mordini, D.; Montalti, M. Effect of Size, Shape and Surface Functionalization on the Antibacterial Activity of Silver Nanoparticles. *J. Funct. Biomater.* **2023**, *14*, 244. [CrossRef]
6. Zhang, M.; Zhu, L.; Wang, J.; Ye, N.; Dai, S.; Yu, S.; Wu, Y. Surface Modification of Biomedical Metals by Double Glow Plasma Surface Alloying Technology: A Review of Recent Advances. *J. Mater. Res. Technol.* **2023**, *24*, 3423–3452. [CrossRef]
7. Wirecka, R.; Maćkosz, K.; Żywczak, A.; Marzec, M.M.; Zapotoczny, S.; Bernasik, A. Magnetoresistive Properties of Nanocomposites Based on Ferrite Nanoparticles and Polythiophene. *Nanomaterials* **2023**, *13*, 879. [CrossRef] [PubMed]
8. Lemine, O.M.; Algessair, S.; Madkhali, N.; Al-Najar, B.; El-Boubbou, K. Assessing the Heat Generation and Self-Heating Mechanism of Superparamagnetic Fe_3O_4 Nanoparticles for Magnetic Hyperthermia Application: The Effects of Concentration, Frequency, and Magnetic Field. *Nanomaterials* **2023**, *13*, 453. [CrossRef]
9. Chernova, E.; Botvin, V.; Galstenkova, M.; Mukhortova, Y.; Wagner, D.; Gerasimov, E.; Surmeneva, M.; Kholkin, A.; Surmenev, R. A Comprehensive Study of Synthesis and Analysis of Anisotropic Iron Oxide and Oxyhydroxide Nanoparticles. *Nanomaterials* **2022**, *12*, 4321. [CrossRef]
10. Jing, H.H.; Bardakci, F.; Akgöl, S.; Kusat, K.; Adnan, M.; Alam, M.J.; Gupta, R.; Sahreen, S.; Chen, Y.; Gopinath, S.C.B.; et al. Green Carbon Dots: Synthesis, Characterization, Properties and Biomedical Applications. *J. Funct. Biomater.* **2023**, *14*, 27. [CrossRef]
11. Mocanu, A.C.; Miculescu, F.; Dascălu, C.A.; Voicu, Ș.I.; Pandele, M.A.; Ciocoiu, R.C.; Batalu, D.; Dondea, S.; Mitran, V.; Ciocan, L.T. Influence of Ceramic Particles Size and Ratio on Surface—Volume Features of the Naturally Derived HA-Reinforced Filaments for Biomedical Applications. *J. Funct. Biomater.* **2022**, *13*, 199. [CrossRef] [PubMed]
12. Yu, L.; Zhu, S.; Qin, K.; Fan, X.; An, L. Macrophages Loaded with Fe Nanoparticles for Enhanced Photothermal Ablation of Tumors. *J. Funct. Biomater.* **2022**, *13*, 94. [CrossRef]
13. Razumova, S.; Brago, A.; Barakat, H.; Howijieh, A.; Senyagin, A.; Serebrov, D.; Guryeva, Z.; Kozlova, Y.; Adzhieva, E. Evaluation of the Microbiological Effect of Colloidal Nanosilver Solution for Root Canal Treatment. *J. Funct. Biomater.* **2022**, *13*, 163. [CrossRef] [PubMed]
14. Li, C.H.; Chan, M.H.; Chang, Y.C.; Hsiao, M. Gold Nanoparticles as a Biosensor for Cancer Biomarker Determination. *Molecules* **2023**, *28*, 364. [CrossRef]
15. Tai, J.; Fan, S.; Ding, S.; Ren, L. Gold Nanoparticles Based Optical Biosensors for Cancer Biomarker Proteins: A Review of the Current Practices. *Front. Bioeng. Biotechnol.* **2022**, *10*, 877193. [CrossRef]
16. Lee, S.; Lee, G.; Jeon, G.; Lee, H.; Park, S.; Sohn, Y.; Park, Y.; Ryu, S. Anti-Aging and Lightening Effects of Au-Decorated Zeolite-Based Biocompatible Nanocomposites in Epidermal Delivery Systems. *J. Funct. Biomater.* **2023**, *14*, 66. [CrossRef]
17. Zamay, T.; Zamay, S.; Luzan, N.; Fedotovskaya, V.; Masyugin, A.; Zelenov, F.; Koshmanova, A.; Nikolaeva, E.; Kirichenko, D.; Veprintsev, D.; et al. Magnetic Nanoscalpel for the Effective Treatment of Ascites Tumors. *J. Funct. Biomater.* **2023**, *14*, 179. [CrossRef]
18. Allafchian, A.; Hosseini, S.S. Antibacterial Magnetic Nanoparticles for Therapeutics: A Review. *IET Nanobiotechnol.* **2019**, *13*, 786–799. [CrossRef]
19. Antonelli, A.; Magnani, M. SPIO Nanoparticles and Magnetic Erythrocytes as Contrast Agents for Biomedical and Diagnostic Applications. *J. Magn. Magn. Mater.* **2022**, *541*, 168520. [CrossRef]
20. Wang, L.; Duan, Y.; Lu, S.; Sun, J. Magnetic Nanomaterials Mediate Electromagnetic Stimulations of Nerves for Applications in Stem Cell and Cancer Treatments. *J. Funct. Biomater.* **2023**, *14*, 58. [CrossRef] [PubMed]
21. Arora, V.; Sood, A.; Kumari, S.; Kumaran, S.S.; Jain, T.K. Hydrophobically Modified Sodium Alginate Conjugated Plasmonic Magnetic Nanocomposites for Drug Delivery & Magnetic Resonance Imaging. *Mater. Today Commun.* **2020**, *25*, 101470. [CrossRef]
22. Michałowska, A.; Żygieło, M.; Kudelski, A. Fe_3O_4-Protected Gold Nanoparticles: New Plasmonic-Magnetic Nanomaterial for Raman Analysis of Surfaces. *Appl. Surf. Sci.* **2021**, *562*, 150220. [CrossRef]
23. Kobylinska, N.; Klymchuk, D.; Khaynakova, O.; Duplij, V.; Matvieieva, N. Morphology-Controlled Green Synthesis of Magnetic Nanoparticles Using Extracts of 'Hairy' Roots: Environmental Application and Toxicity Evaluation. *Nanomaterials* **2022**, *12*, 4231. [CrossRef]
24. Khashan, S.; Dagher, S.; Tit, N.; Alazzam, A.; Obaidat, I. Novel Method for Synthesis of Fe_3O_4@TiO_2 Core/Shell Nanoparticles. *Surf. Coat. Technol.* **2017**, *322*, 92–98. [CrossRef]
25. Noqta, O.A.; Aziz, A.A.; Usman, I.A.; Bououdina, M. Recent Advances in Iron Oxide Nanoparticles (IONPs): Synthesis and Surface Modification for Biomedical Applications. *J. Supercond. Nov. Magn.* **2019**, *32*, 779–795. [CrossRef]
26. Rudayni, H.A.; Shemy, M.H.; Aladwani, M.; Alneghery, L.M.; Abu-taweel, G.M.; Allam, A.A.; Abukhadra, M.R.; Bellucci, S. Synthesis and Biological Activity Evaluations of Green ZnO-Decorated Acid-Activated Bentonite-Mediated Curcumin Extract (ZnO@CU/BE) as Antioxidant and Antidiabetic Agents. *J. Funct. Biomater.* **2023**, *14*, 198. [CrossRef]
27. Bonsignore, G.; Patrone, M.; Martinotti, S.; Ranzato, E. "Green" Biomaterials: The Promising Role of Honey. *J. Funct. Biomater.* **2021**, *12*, 72. [CrossRef] [PubMed]

28. Fatimah, I.; Hidayat, H.; Purwiandono, G.; Khoirunisa, K.; Zahra, H.A.; Audita, R.; Sagadevan, S. Green Synthesis of Antibacterial Nanocomposite of Silver Nanoparticle-Doped Hydroxyapatite Utilizing Curcuma longa Leaf Extract and Land Snail (*Achatina fulica*) Shell Waste. *J. Funct. Biomater.* **2022**, *13*, 84. [CrossRef]
29. Duel, P.; de las Nieves Piña, M.; Morey, J. One-Pot Environmentally Friendly Synthesis of Nanomaterials Based on Phytate-Coated Fe_3O_4 Nanoparticles for Efficient Removal of the Radioactive Metal Ions 90Sr, 90Y and $(UO_2)^{2+}$ from Water. *Nanomaterials* **2022**, *12*, 4383. [CrossRef] [PubMed]
30. Mikhailova, E.O. Gold Nanoparticles: Biosynthesis and Potential of Biomedical Application. *J. Funct. Biomater.* **2021**, *12*, 70. [CrossRef]
31. Longo, R.; Vertuccio, L.; Speranza, V.; Pantani, R.; Raimondo, M.; Calabrese, E.; Guadagno, L. Nanometric Mechanical Behavior of Electrospun Membranes Loaded with Magnetic Nanoparticles. *Nanomaterials* **2023**, *13*, 1252. [CrossRef] [PubMed]
32. Mamani, J.B.; Gamarra, L.F.; De Souza Brito, G.E. Synthesis and Characterization of Fe_3O_4 Nanoparticles with Perspectives in Biomedical Applications. *Mater. Res.* **2014**, *17*, 542–549. [CrossRef]
33. de Jesús Ruíz-Baltazar, Á. Sonochemical Activation-Assisted Biosynthesis of Au/Fe_3O_4 Nanoparticles and Sonocatalytic Degradation of Methyl Orange. *Ultrason. Sonochem.* **2021**, *73*, 105521. [CrossRef] [PubMed]
34. Dheyab, M.A.; Aziz, A.A.; Jameel, M.S.; Khaniabadi, P.M.; Mehrdel, B. Mechanisms of Effective Gold Shell on Fe_3O_4 Core Nanoparticles Formation Using Sonochemistry Method. *Ultrason. Sonochem.* **2020**, *64*, 104865. [CrossRef]
35. Khameneh, B.; Iranshahy, M.; Soheili, V.; Sedigheh, B.; Bazzaz, F. Review on Plant Antimicrobials: A Mechanistic Viewpoint. *Antimicrob. Resist. Infect. Control* **2019**, *6*, 118. [CrossRef] [PubMed]
36. Galai, M.; Rbaa, M.; Ouakki, M.; Dahmani, K.; Kaya, S.; Arrousse, N.; Dkhireche, N.; Briche, S.; Lakhrissi, B.; Ebn Touhami, M. Functionalization Effect on the Corrosion Inhibition of Novel Eco-Friendly Compounds Based on 8-Hydroxyquinoline Derivatives: Experimental, Theoretical and Surface Treatment. *Chem. Phys. Lett.* **2021**, *776*, 138700. [CrossRef]
37. Ren, Z.; Chhetri, A.; Guan, Z.; Suo, Y.; Yokoyama, K.; Lee, S. Structural Basis for Inhibition and Regulation of a Chitin Synthase from *Candida albicans*. *Nat. Struct. Mol. Biol.* **2022**, *29*, 653–664. [CrossRef]
38. Muşat, V.; Crintea, L.; Anghel, E.M.; Stănică, N.; Atkinson, I.; Culiţă, D.C.; Baroiu, L.; Ţigău, N.; Cantaragiu Ceoromila, A.; Botezatu, A.V.; et al. Ag-Decorated Iron Oxides-Silica Magnetic Nanocomposites with Antimicrobial and Photocatalytic Activity. *Nanomaterials* **2022**, *12*, 4452. [CrossRef]
39. Itrat, S.; Naqvi, Z.; Kausar, H.; Afzal, A.; Hashim, M.; Mujahid, H.; Javed, M.; Hano, C.; Anjum, S. Antifungal Activity of Juglans-Regia-Mediated Silver Nanoparticles (AgNPs) against Aspergillus-Ochraceus-Induced Toxicity in In Vitro and In Vivo Settings. *J. Funct. Biomater.* **2023**, *14*, 221.
40. Hashem, A.H.; Saied, E.; Amin, B.H.; Alotibi, F.O.; Al-Askar, A.A.; Arishi, A.A.; Elkady, F.M.; Elbahnasawy, M.A. Antifungal Activity of Biosynthesized Silver Nanoparticles (AgNPs) against Aspergilli Causing Aspergillosis: Ultrastructure Study. *J. Funct. Biomater.* **2022**, *13*, 242. [CrossRef]
41. Dilshad, E.; Bibi, M.; Sheikh, N.A.; Tamrin, K.F.; Mansoor, Q.; Maqbool, Q.; Nawaz, M. Synthesis of Functional Silver Nanoparticles and Microparticles with Modifiers and Evaluation of Their Antimicrobial, Anticancer, and Antioxidant Activity. *J. Funct. Biomater.* **2020**, *11*, 76. [CrossRef] [PubMed]
42. Sobral, R.; Tomasz, A. The Staphylococcal Cell Wall. In *Gram-Positive Pathogens*, 3rd ed.; ASM Press: Washington, DC, USA, 2019; pp. 574–591. [CrossRef]
43. Fosca, M.; Streza, A.; Antoniac, I.V.; Vadalà, G.; Rau, V. Ion-Doped Calcium Phosphate-Based Coatings with Antibacterial Properties. *J. Funct. Biomater.* **2023**, *14*, 250. [CrossRef] [PubMed]
44. Gupta, N.; Gupta, C.; Bohidar, H.B. Visible Laser Light Mediated Cancer Therapy via Photothermal Effect of Tannin-Stabilized Magnetic Iron Oxide Nanoparticles. *Nanomaterials* **2023**, *13*, 1456. [CrossRef]
45. de Jesús Ruíz-Baltazar, Á. Green Synthesis Assisted by Sonochemical Activation of Fe_3O_4-Ag Nano-Alloys: Structural Characterization and Studies of Sorption of Cationic Dyes. *Inorg. Chem. Commun.* **2020**, *120*, 108148. [CrossRef]
46. de Jesus Ruíz-Baltazar, Á. Kinetic Adsorption Models of Silver Nanoparticles Biosynthesized by Cnicus Benedictus: Study of the Photocatalytic Degradation of Methylene Blue and Antibacterial Activity. *Inorg. Chem. Commun.* **2020**, *120*, 108158. [CrossRef]
47. Irfan, H.; Mohamed Racik, K.; Anand, S. Microstructural Evaluation of $CoAl_2O_4$ Nanoparticles by Williamson–Hall and Size–Strain Plot Methods. *J. Asian Ceram. Soc.* **2018**, *6*, 54–62. [CrossRef]
48. Zak, A.K.; Majid, W.A.; Abrishami, M.E.; Yousefi, R. X-ray Analysis of ZnO Nanoparticles by Williamson-Hall and Size-Strain Plot Methods. *Solid State Sci.* **2011**, *13*, 251–256. [CrossRef]
49. Li, D.; Hu, Y.; Wei, H.; Chen, W.; Liu, Y.; Yan, X.; Guo, L.; Liao, M.; Chen, B.; Chai, R.; et al. Superparamagnetic Iron Oxide Nanoparticles and Static Magnetic Field Regulate Neural Stem Cell Proliferation. *Front. Cell. Neurosci.* **2022**, *15*, 583. [CrossRef]
50. Sirgedaite, G.; Talaikis, M.; Niaura, G.; Mikoliunaite, L. Magneto-Plasmonic Nanostructures for SERS: Magnetite Decorated by Silver and Gold Nanoparticles. *New J. Chem.* **2022**, *47*, 402–411. [CrossRef]
51. Romaniuk, J.A.H.; Cegelski, L. Bacterial Cell Wall Composition and the Influence of Antibiotics by Cell-Wall and Whole-Cell NMR. *Philos. Trans. R. Soc. B Biol. Sci.* **2015**, *370*, 20150024. [CrossRef]
52. Trofa, D.; Gácser, A.; Nosanchuk, J.D. Candida Parapsilosis, an Emerging Fungal Pathogen. *Clin. Microbiol. Rev.* **2008**, *21*, 606–625. [CrossRef] [PubMed]
53. Nair Silva-Holguín, P.; de Jesús Ruíz-Baltazar, Á.; Yobanny Reyes-López, S. Antimicrobial Study of the Al_2O_3-Cu and Al_2O_3-Hydroxiapatite-Cu Spheres. *Inorg. Chem. Commun.* **2022**, *138*, 109253. [CrossRef]

54. Estrada-Mata, E.; Navarro-Arias, M.J.; Pérez-García, L.A.; Mellado-Mojica, E.; López, M.G.; Csonka, K.; Gacser, A.; Mora-Montes, H.M. Members of the *Candida parapsilosis* Complex and *Candida albicans* Are Differentially Recognized by Human Peripheral Blood Mononuclear Cells. *Front. Microbiol.* **2016**, *6*, 1527. [CrossRef]
55. Salama, A.; Saleh, A.K.; Cruz-Maya, I.; Guarino, V. Bacterial Cellulose/Cellulose Imidazolium Bio-Hybrid Membranes for In Vitro and Antimicrobial Applications. *J. Funct. Biomater.* **2023**, *14*, 60. [CrossRef]
56. D'Orto, B.; Chiavenna, C.; Leone, R.; Longoni, M.; Nagni, M.; Capparè, P. Marginal Bone Loss Compared in Internal and External Implant Connections: Retrospective Clinical Study at 6-Years Follow-Up. *Biomedicines* **2023**, *11*, 1128. [CrossRef] [PubMed]
57. Qi, M.; Chi, M.; Sun, X.; Xie, X.; Weir, M.D.; Oates, T.W.; Zhou, Y.; Wang, L.; Bai, Y.; Xu, H.H.K. Novel Nanomaterial-Based Antibacterial Photodynamic Therapies to Combat Oral Bacterial Biofilms and Infectious Diseases. *Int. J. Nanomed.* **2019**, *14*, 6937–6956. [CrossRef] [PubMed]
58. Chi, M.; Li, N.; Cui, J.; Karlin, S.; Rohr, N.; Sharma, N.; Thieringer, F.M. Biomimetic, Mussel-Inspired Surface Modification of 3D-Printed Biodegradable Polylactic Acid Scaffolds with Nano-Hydroxyapatite for Bone Tissue Engineering. *Front. Bioeng. Biotechnol.* **2022**, *10*, 1646. [CrossRef] [PubMed]
59. Li, W.; Qi, M.; Sun, X.; Chi, M.; Wan, Y.; Zheng, X.; Li, C.; Wang, L.; Dong, B. Novel Dental Adhesive Containing Silver Exchanged EMT Zeolites against Cariogenic Biofilms to Combat Dental Caries. *Microporous Mesoporous Mater.* **2020**, *299*, 110113. [CrossRef]